

## EFFECT ON STRUCTURAL AND OPTICAL PROPERTIES OF Zn-SUBSTITUTED COBALT FERRITE $\text{CoFe}_2\text{O}_4$

M. T. JAMIL<sup>a\*</sup>, J. AHMAD<sup>a</sup>, S. H. BUKHARI<sup>a</sup>, T. SULTAN<sup>b</sup>, M. Y. AKHTER<sup>c</sup>,  
H. AHMAD<sup>d</sup>, G. MURTAZA<sup>e</sup>

<sup>a</sup>Department of Physics, Bahauddin Zakariya University Multan 60800, Pakistan.

<sup>b</sup>Department of Civil Engineering, Bahauddin Zakariya University Multan 60800, Pakistan.

<sup>c</sup>Department of Physics, University of Sargodha Lyallpur Campus Faisalabad 38000, Pakistan.

<sup>d</sup>Nanoscience and Technology Department, National Center for Physics, Quaid-i-Azam University Campus, Islamabad 45320, Pakistan.

<sup>e</sup>Department of Physics, GC University Faisalabad, Layyah Campus, Layyah 31200, Pakistan.

A series of spinel ferrites with composition  $\text{Zn}_x\text{Co}_{1-x}\text{Fe}_2\text{O}_4$  ( $0 \leq x \leq 1$ ) has been synthesized via co-precipitation route. The samples have been characterized by means of X-ray diffraction (XRD), Scanning electron microscope (SEM), Fourier transform infrared (FTIR) spectroscopy, UV-visible spectroscopy and Photoluminescence (PL) spectroscopy. X-ray diffraction (XRD) technique was applied to characterize the nanoparticles. The particle size of the obtained samples was calculated by using Sherrer's formula were found in the range of (30 to 70 nm) on annealing at 700 °C. The scanning electron microscope was used to study the morphology of the synthesized samples which revealed the heterogeneous grain size distribution. FTIR transmittance spectroscopy was used to investigate the bonding among different atoms present in the sample. The frequency bands near  $564\text{-}588\text{cm}^{-1}$  and  $425\text{-}442\text{cm}^{-1}$  are assigned to the tetrahedral and octahedral clusters which confirm the presence of metal oxygen (M-O) stretching band in ferrites. UV-visible spectroscopy was used to calculate optical energy band gap by using Tauc relation.

(Received November 30, 2016; Accepted February 20, 2017)

*Keywords:* X-ray diffraction, FTIR, Photoluminescence (PL), Cobalt ferrite.

### 1. Introduction

Recently, attention in nano-sized spinel ferrites has significantly increased due to their importance in understanding the fundamentals in nano magnetism [1]. Ferrite with remarkable magnetic and micro wave absorbing properties has been widely used in the fields of data storage devices, magnetic sensors, actuators, bio-technology, and audio tapes [2]. Ferrite properties strongly depend on the chemical composition, cation distribution, sintering temperature and time, additive amount of the cations and methods of preparation. The soft magnetic behavior in ferrites is caused by the exchange interaction among the cations on the polyhedral sites. The rare earth cations having their 4f orbital which play a key role in the electrical and magnetic properties of ferrites [3]. From bulk material to nanoscale level magnetic properties of ferrites changes, consequently bulk zinc ferrite is anti-ferromagnetic then it turns to ferromagnetic or super paramagnetic as size of particle reduces at nano scale [4-7]. Now a day's family of spinel ferrites with chemical formula  $\text{MFe}_2\text{O}_4$  (where M represents divalent ions of the transition metal elements such as Ni, Cu, Co, Zn, Mg and Mn etc.) are widely used at commercial level due to their excellent magnetic and electrical properties. On the base of metal ions distribution at A and B sites there are three types of spinel ferrites namely normal, inverse and random. Spinel ferrites possess cubic

---

\*Corresponding author: tufiqjamil@yahoo.com

structure. There are 8 molecules in unit cell of the spinel structure. In that cubic cell, 32 octahedral and 64 tetrahedral sites are available but out of them only 16 octahedral and 8 tetrahedral sites occupied by metal ions [8-9].  $\text{ZnFe}_2\text{O}_4$  have spinel structure with tetrahedral sites occupied by zinc ions ( $\text{Zn}^{2+}$ ) and octahedral sites by iron ions ( $\text{Fe}^{3+}$ ) respectively [10]. Properties of ferrites are highly sensitive to their synthesis methods, synthesis parameters, nature of substitutions and their compositions. So for there are many synthesis strategies for spinel ferrites such as hydrothermal, co-precipitation and sol gel method etc [5]. Recently Lopez et.al [11] synthesized zinc doped cobalt ferrites nanoparticles via co-precipitation method. They claimed that as Zn concentration increases, the particle size and coercive field decreases gradually. Ghasemi et.al [12-13] synthesized  $\text{Zn}_{1-x}\text{Co}_x\text{Fe}_2\text{O}_4$  nanoparticles powder via sol-gel method and demonstrated that by increasing cobalt concentration magnetic properties changes from paramagnetic to ferromagnetic. They also concluded that increment of cobalt content in  $\text{ZnFe}_2\text{O}_4$  enhanced saturation magnetization and coercivity. There has been lot of work done towards  $\text{CoFe}_2\text{O}_4$  side, but serious lack of systematic investigations in  $\text{Zn}_x\text{Co}_{1-x}\text{Fe}_2\text{O}_4$  system towards  $\text{ZnFe}_2\text{O}_4$  sides [14]. Hence an interesting aspect to study such types of system our current research work is the synthesis of  $\text{Zn}_x\text{Co}_{1-x}\text{Fe}_2\text{O}_4$  nanoparticles with interval 0.2 ( $0 \leq x \leq 1$ ) by using co-precipitation technique. Our main focus is to investigate the structural properties of whilst ferrites. The X-ray diffraction pattern and microstructure of prepared nanomaterials are discussed as function of Zinc content.

## 2. Materials and methods

All the chemicals were purchased from Sigma Chemicals USA and were used without extra purification (99.9% purity). Chemicals used in the synthesis were ( $\text{CoCl}_2 \cdot 6\text{H}_2\text{O}$ ,  $\text{ZnCl}_2$ ,  $\text{FeCl}_3 \cdot 6\text{H}_2\text{O}$  and  $\text{NaOH}$ ). For synthesis of  $\text{Zn}_x\text{Co}_{1-x}\text{Fe}_2\text{O}_4$  nanoparticles, 0.5M solution of  $\text{CoCl}_2 \cdot 6\text{H}_2\text{O}$  and 0.5M of  $\text{ZnCl}_2$  were prepared in 50 ml deionized water, separately. A 1M solution  $\text{FeCl}_3 \cdot 6\text{H}_2\text{O}$  was also prepared in 50mL deionized water. Solutions of  $\text{CoCl}_2 \cdot 6\text{H}_2\text{O}$  and  $\text{ZnCl}_2$  were subsequently mixed in  $\text{FeCl}_3 \cdot 6\text{H}_2\text{O}$  solution. A homogeneous solution was obtained by stirring both solutions over a hot-plate at  $65^\circ\text{C}$  and moderate speed (60 rpm) for 30 min. A base solution of 3.5M  $\text{NaOH}$  was used to adjust the pH of solution at 10. During drop wise addition of base solution, homogeneous solution was continuously stirred. It took around 120 min until a reddish brown precipitates were formed. For the refinement of the structure of nanoparticles, thermal decomposition of chlorides of cobalt, zinc, and iron was done. Subsequently synthesized nanoparticles were cooled to room temperature and digestion was performed for 120 minutes to get settle the particles at the bottom of the beaker. Grade 520A filter paper of nano sized pore was used for filtration of  $\text{Zn}_x\text{Co}_{1-x}\text{Fe}_2\text{O}_4$  precipitate. Consequently acquired precipitates were washed several time with de ionized water and ethanol so that the chlorides were removed completely and the pH of residual solution reached to 7. The sample was placed in an oven (18EG Lab. Oven USA) and dried at  $100^\circ\text{C}$  for 4 h [15]. Fine powder was obtained by grinding of dried sample with the help of pestle and mortar and then calcination was performed in a muffle furnace (Tanur Vulcan Muffle Furnace Digital D550 USA) at  $700^\circ\text{C}$  for 3 h.

### 2.1. Characterizations

$\text{Zn}_x\text{Co}_{1-x}\text{Fe}_2\text{O}_4$  formation was confirmed by the XRD with  $\text{Cu K}\alpha$  ( $\lambda=1.5405\text{\AA}$ ) results. Scanning electron microscope (JEOL JSM6360 USA) was used to study overall morphology of nanoparticles and a gold coated specimen was used for this purpose. For the study of functional group FTIR analysis was performed. Furthermore UV-Vis-NIR spectrophotometer at room temperature was used to study the UV-Vis absorption spectra.

### 2.2. Calculations

The structural parameters such as lattice constant ( $a$ ), unit cell volume ( $V_{\text{cell}}$ ), crystallite size ( $D$ ), bulk density, X-ray density and porosity were calculated from XRD data using the following formulae [16-17].

$$a = \frac{\lambda}{2\sin\theta} \sqrt{h^2 + k^2 + l^2} , \quad (1)$$

$$V_{\text{cell}} = a^3, \quad (2)$$

$$D = \frac{k\lambda}{B_{(hkl)}\cos\theta}, \quad (3)$$

$$\rho_{\text{X-ray}} = \frac{ZM}{N_A V}, \quad (4)$$

Here ‘a’ is lattice constant, (hkl) are Miller indices, V is the unit cell volume, Z represents 8 molecules per unit cell of the spinel structure,  $N_A$  is the Avogadro’s number and M is the molecular weight of the sample. Scherer’s formula ascribed by Eq. 3 was used to calculate the crystallite size (D) nm, where K is the shape factor,  $\lambda$  is the X-ray wavelength and  $\theta$  is the Bragg’s diffraction angle and  $B_{(hkl)}$  is the integral width (defined as the peak area divided by peak height) of peak in radian.

### 3. Results and discussions

#### 3.1. Crystal Structure Analysis

The X-ray diffraction patterns of  $\text{CoZnFe}_2\text{O}_4$  nanoparticles calcined at 700 °C revealed highly crystalline and intense diffraction peaks corresponding to simple cubic structure. Some minor phases were also present. Well defined peaks are (220), (311), (400), (511) and (440) of spinel structure can be observed in the Fig.1. The strongest reflection of (311) plane represent cubic spinel structure. As minor phases, additional peaks of ZnO, hematite [18-20] and CoO was also be observed.

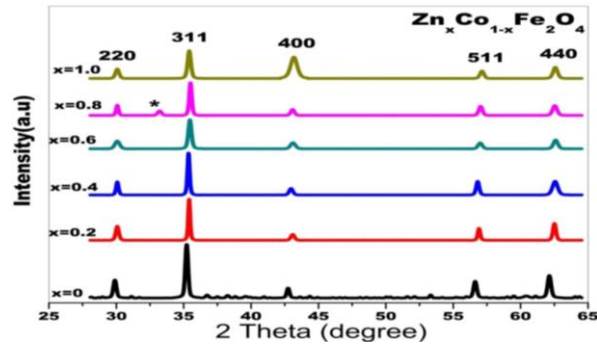


Fig.1 XRD pattern of  $\text{Zn}_x\text{Co}_{1-x}\text{Fe}_2\text{O}_4$  ferrites ( $0 \leq x \leq 1$ ) at 700 °C for 3 h.

Table 1. Lattice constant, volume of the unit cell, crystallite size (nm), X-ray density ( $D_x$ ) of Zn substituted Co-ferrites annealed at temperature 700 °C for 3 h.

| Composition/FW  | Lattice constant<br>a (Å) | Volume of the<br>unit cell (Å <sup>3</sup> ) | Crystallite size<br><D>(nm) | X-ray density<br>$D_x$ (g/cm <sup>3</sup> ) |
|---|---------------------------|--|-----------------------------|---|
| $\text{CoFe}_2\text{O}_4$ (234.623)                             | 8.3765                    | 587.75                                       | 21.2                        | 5.26  |
| $\text{Zn}_{0.2}\text{Co}_{0.8}\text{Fe}_2\text{O}_4$ (235.912) | 8.4089                    | 594.58                                       | 35.3                        | 5.27  |
| $\text{Zn}_{0.4}\text{Co}_{0.6}\text{Fe}_2\text{O}_4$ (237.202) | 8.4081                    | 594.41                                       | 30.2                        | 5.30  |
| $\text{Zn}_{0.6}\text{Co}_{0.4}\text{Fe}_2\text{O}_4$ (238.781) | 8.3996                    | 592.61                                       | 20.2                        | 5.39  |
| $\text{Zn}_{0.8}\text{Co}_{0.2}\text{Fe}_2\text{O}_4$ (239.781) | 8.3865                    | 589.86                                       | 20.1                        | 5.40  |
| $\text{ZnFe}_2\text{O}_4$ (241.07)                              | 8.4175                    | 569.41                                       | 30.3                        | 5.37  |

### 3.2. FT-IR Spectrum Analysis

Fig.2 shows the FTIR spectra of representative sample  $Zn_{0.6}Co_{0.4}Fe_2O_4$  that were recorded in the range of  $500-4000\text{ cm}^{-1}$ . The common features of ferros spinel ferrites spectra exhibit bands below  $1000\text{ cm}^{-1}$  are metal oxygen (M-O) vibration mode. These spectra represent characteristic features of spinel ferrites. It has been observed that the high frequency band lies in the range  $524-579\text{ cm}^{-1}$ . There is not found any kind of other group peaks which meant that the synthesized material finger print free from organic compounds. The absorption bands are assigned to metal oxygen stretching frequencies. The observed stretching frequency is expected to appear at higher frequency compared to the M-O stretching frequency of octahedral (Oh M-O) sites [21]. According to Waldron [22] the vibrations of the unit cell of cubic spinel can be constructed in the tetrahedral site and octahedral site. Meanwhile, it can be seen that the bands frequency shifts slightly towards higher frequency side from  $530.06-533.86\text{ cm}^{-1}$ ,  $538.09-537.88\text{ cm}^{-1}$ . These recorded values of the spectra identified as the (M-O) metal oxygen stretching vibrations of the spinel ferrite. Thus, the replacement of Fe ions with Cobalt ions at octahedral sites have different ionic radius and atomic mass, is the important reason of the observed shift in the band position.

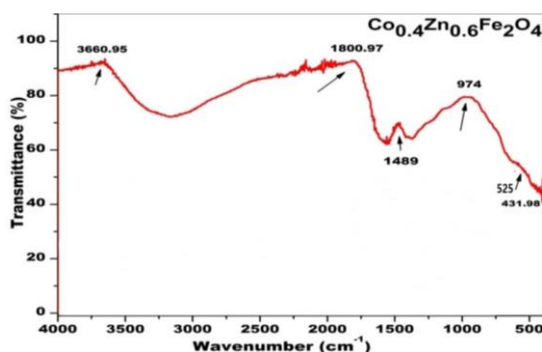


Fig.2 FT-IR Spectra of Zn-substituted Co-ferrites at  $x = 0.6$ .

### 3.3 Morphology analysis

Fig.3(a-d) shows the morphology of Zn-substituted Co ferrites (with  $x = 0.2, 0.4, 0.6$  and  $0.8$ ) at annealing temperatures  $700\text{ }^{\circ}\text{C}$  for 3 h by co-precipitation method. It is observed that surface of the images of pallets is appeared roughly not a smooth surface. The compact pallet reveals that the heterogeneous grain size distribution. It is noteworthy that the recorded images that taken without any gold coating. The surface morphology shows that the shape of the synthesized material approximately uniform in micron size determined by line intercepts method. Moreover, it is observed that the grain size decreases with the increase of Zn substitution in the Co-ferrite.

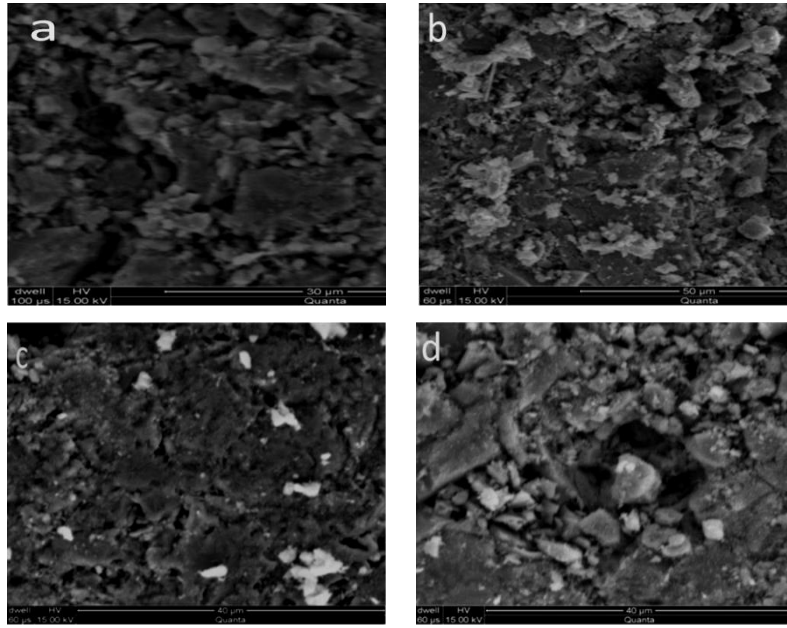


Fig.3 Micrographs of Zn-substituted Co-ferrites at  $x= 0.2, 0.4, 0.6$  and  $0.8$ .

### 3.4 Optical characteristic

The energy band gap of the material is determined by using UV-visible spectra according to Tauc relation [23],

$$\alpha h\nu = A(h\nu - E_g)^n, \quad (5)$$

Where  $E_g$  the energy gap, constant  $A$  is different for different transitions,  $(h\nu)$  is the energy of the photon and  $n$  is an index which assumes the value  $1/2, 3/2, 2$  and  $3$  depending on the nature of the electronic transition responsible for the reflection. The value of  $n$  is  $1/2$  for allowed and  $2$  for forbidden direct energy gap for ferrites [24]. Further, the value of  $\alpha$  has been calculated by the following relation,

$$\alpha = 4\pi k/\lambda, \quad (6)$$

where  $\lambda$  is wavelength in nm and  $k$  is absorption index.

The optical band gap and the absorption coefficient of the synthesized ferrites were calculated by Eq. (5 and 6), respectively [25]. Fig.4 illustrates the UV-visible absorbance spectra of the Zn substituted Co ferrites, the absorbance decreases as the doping of Zn. Fig. 4 (a) shows at  $x = 0$ , the absorption is maximum but at  $x = 1$ , the absorption is very low. For the other four different concentrations *i.e.* (at  $x = 0.2, 0.4, 0.6, 0.8$ ) absorption is very near to each other but at lower wavelength its value is high. But the general trend for all the six curves shows the same behavior. The similar trend has also been observed for  $\ln\alpha$  in Fig. 4 (b).

The absorption coefficient  $\alpha$  is related to extinction coefficient  $K$  by [26],

$$K = \frac{\alpha\lambda}{4\pi}, \quad (7)$$

The Reflectance ( $R$ ) is be written as in term of refractive index ( $n$ ) [27] as,

$$R = \frac{(n-1)^2}{(n+1)^2}, \quad (8)$$

It can also be written in terms of absorption coefficient as,

$$R = \frac{1 \mp \sqrt{1 - \exp(-at + \exp(at))}}{1 + \exp(-at)}, \quad (9)$$

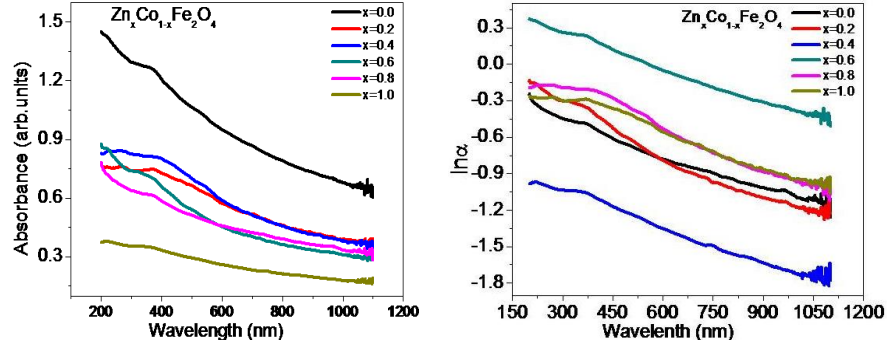


Fig. 4. (a) UV spectrum absorption (b) absorbance coefficient  $\ln(\alpha)$  of the Zn-substituted Co-ferrites.

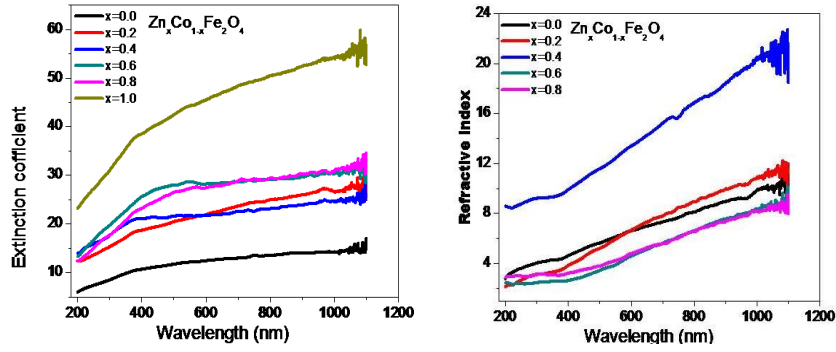


Fig.5 (a) Extinction coefficient (b) Refractive index of the Zn-substituted Co-ferrites.

From the above equation, the refractive index  $n$  can be derived as,

$$n = -\frac{(R+1) \mp \sqrt{3R^2 + 10R - 3}}{2(R-1)}, \quad (10)$$

Fig. 5(a) shows the plot of extinction coefficient ( $K$ ) as a function of wavelength. It shows at  $x = 1$ , the extinction coefficient is maximum but at  $x = 0.0$ , the extinction coefficient is very low. For the other four different concentrations *i.e.* ( $x = 0.2, 0.4, 0.6, 0.8$ ) are very near to each other. For higher wavelength, plot shows the high value of extinction coefficient, but the general trend for all the six curves of the extinction coefficient shows the same behavior with spectral dependence. The dependence of the refractive index ( $n$ ) with the wavelength is shown in Fig. 5(b). For lower wavelength, plot shows the lower values of the refractive index, but the general trend for all the six curves shows the same behavior with wavelength.

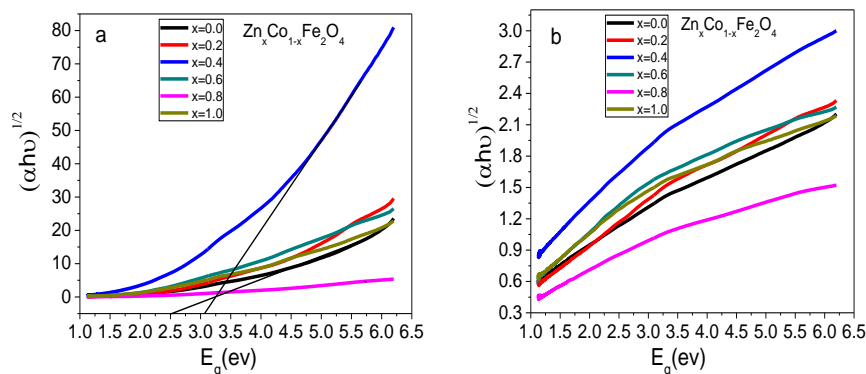


Fig.6. (a) Plots  $(\alpha h\nu)^2$  Vs Photon energy (eV) and (b)  $(\alpha h\nu)^{1/2}$  Vs Photon energy (eV).

The value of optical energy band gap ( $E_g$ ) has been calculated for the all samples by  $(\alpha h\nu)^2$  vs.  $h\nu$  plots see Fig. 6(a). The values of  $E_g$  for different samples were found by extrapolating the linear portion to the  $h\nu$  (i.e.  $\alpha = 0$ ) determine the energy band gap  $E_g$  to be vary 2.5 eV to 3.1 eV. It is observed that by increasing the concentration of the Zn band gap increases. Due to such variations structural changes occur into the composition. The allowed direct band gap transition for n is 1/2 is shown in Fig. 6(b).

### 3.5. Photoluminescence spectra

Photoluminescence (PL) spectroscopy is an excellent technique to obtain useful information about energy as well as dynamics of charge carriers produced during the exposure of light. PL behavior of spinel ferrites nanoparticles yields information on the energies and dynamics of photo generated charge carriers as well as on the nature of the emitting states. Electron from ferrite sample lies in the conduction band, excitonic states and trap states [28-32]. It is well known that emission and efficiency are very sensitive to nature of nanoparticles surface, due to the presence of gap surface states arising from surface non-stoichiometry and unsaturated bonds. Surface trap states allow non-radioactive recombination and enhance luminescence efficiency. In spinel ferrites, electrons are present in trap states, excitonic states and conduction bands [33]. The Photoluminescence (PL) spectrum of Zn<sub>0.4</sub>Co<sub>0.6</sub>Fe<sub>2</sub>O<sub>4</sub> ferrite at room temperature is presented in Fig. 7. In the spectrum of the sample the broad emission peak with energy 0.33 eV is attributed to the charge recombination which is due to the lattice defects and deep traps of localized surface states [34]. These defects in the lattice of nanomaterial are the basis of luminescent properties. Moreover, photoluminescence (PL) peak is attributed to the recombination of charge carriers in deep traps of surface localized states and lattice defects [35-37]. Therefore such defects are responsible for the luminescent properties of the synthesize nanomaterials. In this manner, the spectral position and yield of the crystallite fluorescence can be modified by changing the chemical nature of the colloid surface. Hence it has observed that the higher wavelength peak may come due to some impurity in our material. The presence of defects in the nanoparticle was also supported by the SEM images of the sample (Fig.3).

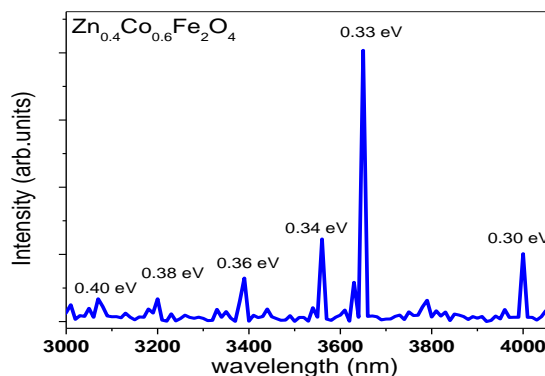


Fig.7. Photoluminescence (PL) spectra of the represented sample at room temperature.

#### 4. Conclusions

A series of polycrystalline Zn-substitution Co-ferrites system ( $\text{Zn}_x\text{Co}_{1-x}\text{Fe}_2\text{O}_4$  where  $0.0 \leq x \leq 0.10$  with interval 0.2) synthesized by co-precipitation technique and sintered at  $700^\circ\text{C}$  for 3 h. The effect of Zn-content on the structural parameters has been studied. X-ray diffraction confirmed that the high degree of order and mono dispersity of the nanoparticles that exhibits the single phase face center cubic structure (FCC).

The physical parameters of the material revealed that the crystallite size were found in the range (30-70 nm) while lattice parameter, X-ray density decreases with the increase of Zn-concentrations. SEM revealed that the synthesized samples have heterogeneous grain size distribution. The energy band gap  $E_g$  is in the range of 2.5 eV to 3.1 eV for prepared samples. The frequency bands near  $525\text{ cm}^{-1}$  and  $924\text{ cm}^{-1}$  are assigned to the tetrahedral and octahedral clusters which confirm the presence of M-O stretching band in ferrites. So the degree of quantum confinement in these spinel ferrites was determined from their optical absorption and photoluminescence spectra.

#### References

- [1] T. E. Quickel, V. H. Le, T. Brezesinski, S. H. Tolbert, *Nano Lett.* **10**, 2982 (2010).
- [2] J. C. Wacrenborg, M. O. Figuerido, J. M. P. Cabrol, L. C. J. Pereira, *J. Solid State Chem.* **111**, 300 (1994).
- [3] P. C. Rajath, R. S. Manna, D. Banerjee, M. R. Varma, K. G. Suresh, A. K. Nigam, *J. Alloy Comp.* **453**, 298 (2008).
- [4] I. Sharifi, H. Shokrollahi, S. Amiri, *J. Magn. Magn. Mater.* **324**, 903 (2012).
- [5] M. Liangruksa, R. Ganguly, I. K. Puri, *J. Magn. Magn. Mater.* **323**, 708 (2011).
- [6] H. B. Na, I. C. Song, T. Hyeon, *Adv. Mater.* **21**, 2133 (2009).
- [7] M. Mahmoudi, S. Sant, B. Wang, S. Laurent, T. Sen, *Adv. Drug Deliv. Rev.* **63**, 24 (2010).
- [8] W. Jiangtao, N. Li, JunXu, Y. Jiang, Z. Guang Ye, X. Zhaoxiong, L. Zheng, *Appl. Phys. Lett.* **99**, 202505 (2011).
- [9] A. Manikandan, L. J. Kennedy, M. Bououdina, J. J. Vijaya, *J. Magn. Magn. Mater.* **349**, 249 (2014).
- [10] S. C Goh, C. H. Chia, Zakaria, S. Yusoff, M. Haw, C. Y. S. Ahmadi, N. M. Huang, H. N. Lim, *Material Chemistry and Physics* **120**, 31 (2010).
- [11] M. Veverka, Z. Jirák, O. Kaman, K. Knížek, M. Maryško, E. Pollert, K. Závěta, A. Lančok, M. Dlouhá, S. Vratislav, *Nanotechnology* **22**, 345701 (2011).

- [12] A. Ghasemi, V. Sepelak, S. E. Shirsath, X. Liu and A. Morisako, *J. Appl. Phys.* **109**, 07A512 (2011).
- [13] A. Sharma, K. Parmar, R. K. Kotnala, N. S. Negi, *International J. Adv. Engg. Tech.* **5**, 544 (2012).
- [14] M. H. Yousefi, S. Manouchehri, A. Arab, M. Mozaffari, G. RAmiri, *Mater Res Bull* **45**, 1792 (2010).
- [15] E. Casbeer, V. K. Sharma, X. Z. Li, *Separation and Purification Technology* **87**, 1 (2012).
- [16] B.D. Cullity, *Second Edition Addison Wesley Publishing* **42-46** (89), 92 (1978).
- [17] G. Mustafa, M. U. Islam, W. Zhang, Y. Jamil, A. W. Anwar, M. Hussain, M. Ahmad, *J. Alloys Comp* **618**, 428(2015).
- [18] B. D. Cullity, *Elements of X-Ray Diffraction*. (2nd edtn), Reading, MA: Addison Wesley. (1978).
- [19] S. Kumar, V. Singh, S. Aggarwal, U. K. Mandal, R. K. Kotnala, *J. Magn. Magn. Mater.* **324**, 3683 (2012).
- [20] O. Perales, O. N. C. Uwakweh, C. Osorio, H. A. Radovan, *J. Appl. Phys* **109**, 07C324 (2011).
- [21] R. A. Smith, *Semiconductors*, Cambridge University Press, London, 2nd edn. (1978).
- [22] Waldron, J. Conor, N. J. English, *Chemical Physics Letters* **649**, 119 (2016).
- [23] J. Tauc, R. Grigorovici, Vancu, *physica status solidi (b)* **15**(2) 627 (1966).
- [24] N. Orhan, M. Baykul, *Solid State Electron.* **78**, 147 (2012).
- [25] D. E. Skinner, D. P. Colombo, J. J. Cavaleri, R. M. Bowman, *J. Phys. Chem.* **99**, 7853 (1995).
- [26] R. E. Denton, R. D. Campbell, S. G. Tomlin, *J. Phys. D* **5**, 852 (1972).
- [27] A. Ashour, N. E. Kadry, S. A. Mahmoud, *Thin Solid Films* **269**, 117 (1995).
- [28] T.W. Roberti, N. J. Cherepy, J. Z. Zhang, *J. Chem. Phys.* **108**, 2143 (1998).
- [29] M. C. Brelle, J. Z. Zhang, *J. Chem. Phys.* **108**, 3119 (1998).
- [30] N. J. Cherepy, D. B. Liston, J. A. Lovejoy, H. M. Deng, J. Z. Zhang, *J. Phys. Chem. B* **102**, 770 (1998).
- [31] M.C. Brelle, J. Z. Zhang, L. Nguyen, et. al. *J. Phys. Chem. A* **103**, 10194 (1999).
- [32] A. Sengupta, B. Jiang, K. C. Mandal, et. al. *J. Phys. Chem. B* **103**, 3128 (1999).
- [33] D. E. Skinner, D. P. Colombo, J. J. Cavaleri, R. M. Bowman, *Femtosecond, The Journal of Physical Chemistry* **99** (20), 7853 (1995).
- [34] A. Sengupta, B. Jiang, K. Mandal, J. Zhang, *The Journal of Physical Chemistry B* **103** (16), 3128 (1999).
- [35] U. Resch, A. Eychmuller, M. Hasse, H. Wellner, *Langmuir* **8**, 2215 (1992).
- [36] Y. Lin, J. Zhang, E. H. Sargent, E. Kumacheva, *Appl. Phys. Lett.* **81**, 3134 (2002).
- [37] N. Chestoy, T. D. Harris, R. Hull, L.E. Brus, *J. Phys. Chem.* **90**, 3393 (1986).